CHAPTER 2

Experimental Techniques and Details: Degenerate Four Wave Mixing and Z-scan

This chapter presents the details of the experimental techniques employed for different studies carried out. A brief introduction to Degenerate Four Wave Mixing (DFWM) and Z-scan techniques, their applicability to dynamics and nonlinear absorption studies is given. The complete details of the experimental set-up for both the techniques, using different configurations, are highlighted. A brief introduction to the photo-physics of a typical organic molecule is presented. Our initial DFWM results on the samples Rhodamine B (RhB) and CS_2 using the incoherent light are also presented.

2.1 Introduction

The magnitude and response of third-order nonlinear susceptibility are important parameters in characterising and determining the applicability of any material as a nonlinear optical device. There are several techniques [1-7] for measuring these parameters that include

(a) **Degenerate Four Wave Mixing**: For measurement of both magnitude and response time of the third-order nonlinearity
(b) **Third Harmonic Generation**: For measurement of magnitude of third-order nonlinearity only.
(c) **Z-scan**: For measurement of sign, magnitude of third-order nonlinearity.
(d) **Electro-Absorption technique**: Dispersion studies of third-order nonlinearity
(e) **Time-resolved Optical Kerr Effect and Transient Absorption techniques**: For the study of photo-physical processes determining the nonlinearity.

Among these DFWM is one of the most important and versatile technique, which provides information about the magnitude and response of the third-order nonlinearity. In this process, three coherent beams incident on a nonlinear medium generate a fourth beam due to the third order nonlinearity. The strength of this fourth beam is dependent on a coupling constant that is proportional to effective $\chi^{(3)}$ and hence measurements on PC signal will yield information about the $\chi^{(3)}$ tensor components of the medium [8-

16]. DFWM can be employed in backward (or generally called the Phase Conjugate), forward or boxcar configurations, with the choice on the experimental conditions and the requirements. Using different polarizations of the three beams it is possible to measure all the independent $\chi^{(3)}$ tensor components of an isotropic material. Some of the several advantages of this technique being

- The Phase Conjugate signal is distinguishable from others by simple spatial separation.
- The detected signal has a characteristic dependence on the input intensities, which can be used for verification of the experiment.
- The sample could be in any form (isotropic) and all the independent tensor components of $\chi^{(3)}$ can be measured in a single experiment.
- Beams other than true Gaussian modes can be employed.
- The time dependence of the probe beam gives information about the response times of the nonlinearity.

2.1.1 Degenerate Four Wave Mixing (DFWM)

A Four Wave Mixing experiment can also be considered as an interaction of three optical fields in a medium. The presence of a third-order optical nonlinear susceptibility $\chi^{(3)}$ leads to the creation of various components of material polarisation, giving rise to new optical fields. If the phase-matching condition is fulfilled (i.e. the phase relation between the waves emitted by different parts of the nonlinear medium leads to constructive build up of the resulting wave), new beams of light are created. If the fields are of identical frequencies, the process is termed as Degenerate Four Wave Mixing and the output beam will have the same frequency. The time resolution of the FWM measurements depends on two parameters. The first is related to the time duration of the laser pulses and the second is related to the coherence time of the laser pulses.

The whole process can be looked in another way and treating it as creation of the transient gratings by interference of pairs of waves and Bragg diffraction of the

other wave from the grating formed in the material by it's nonlinear response to spatially modulated light intensity. At the crossing of two beams, the spatial modulation of their electric fields varies due to constructive and destructive interference. The molecules in the interaction region experience varying electric field intensities according to their position and this leads to the formation of a transient grating of polarised molecules in space. The formation of the grating does not require that the two crossing beams coincide in time as long as the coherence is maintained in the sample. Based on the relative timing of the three fields one can envision different gratings formed as shown in fig. 2.1 [1]. The grating formed by $\mathbf{k_1}$ and $\mathbf{k_2}$ waves gets diffracted by $\mathbf{k_3}$ beam to yield the output at $\mathbf{k_3} \pm (\mathbf{k_1} - \mathbf{k_2})$. The one formed by $\mathbf{k_2}$ and $\mathbf{k_3}$ gets diffracted by $\mathbf{k_1}$ to yield the output at $\mathbf{k_1} \pm (\mathbf{k_2} - \mathbf{k_3})$. They are illustrated in the fig. 2.1 for the special case of $\mathbf{k_1} = -\mathbf{k_2}$. The output waves are expected in the directions $-\mathbf{k_3}$ and $\mathbf{k_3} \pm \mathbf{k_1}$. The generation of output in $-\mathbf{k_3}$ direction is phase-matched, and is known as phase conjugate signal, while in the $\mathbf{k_3} \pm \mathbf{k_1}$ directions is not. Thus usually only the output at $\mathbf{k_4} = -\mathbf{k_3}$ needs to be considered.

In the phase conjugate configuration, the backward pump is delayed with respect to other to observe the decay of the grating. For small values of θ the grating 'written' by the forward pump and probe pulses will have a large spatial period $\Lambda = \lambda/(2n_0 \mathrm{Sin}(\theta/2))$. When the pulses coincide in time two other gratings are also formed, a small period grating generated by the interaction of the backward pump and the probe pulses and a two-photon temporal coherence grating. However the spacing of the small-period grating (given now by $\Lambda = \lambda/(2n_0 \mathrm{Sin}((\pi - \theta)/2))$ is considerably smaller than the large-period one. In our case the spacing of the large-period grating is found to be ~ 2 - 3 μ (depending on the angle θ and the refractive index of the solvent) and for the small-period grating it is calculated to be 0.2 – 0.3 μ. If diffusive processes are present the small-period grating washes out rapidly. The contribution of the two-photon grating is usually negligible, and can be observed under special conditions of strong enhancement due to two-photon resonance.

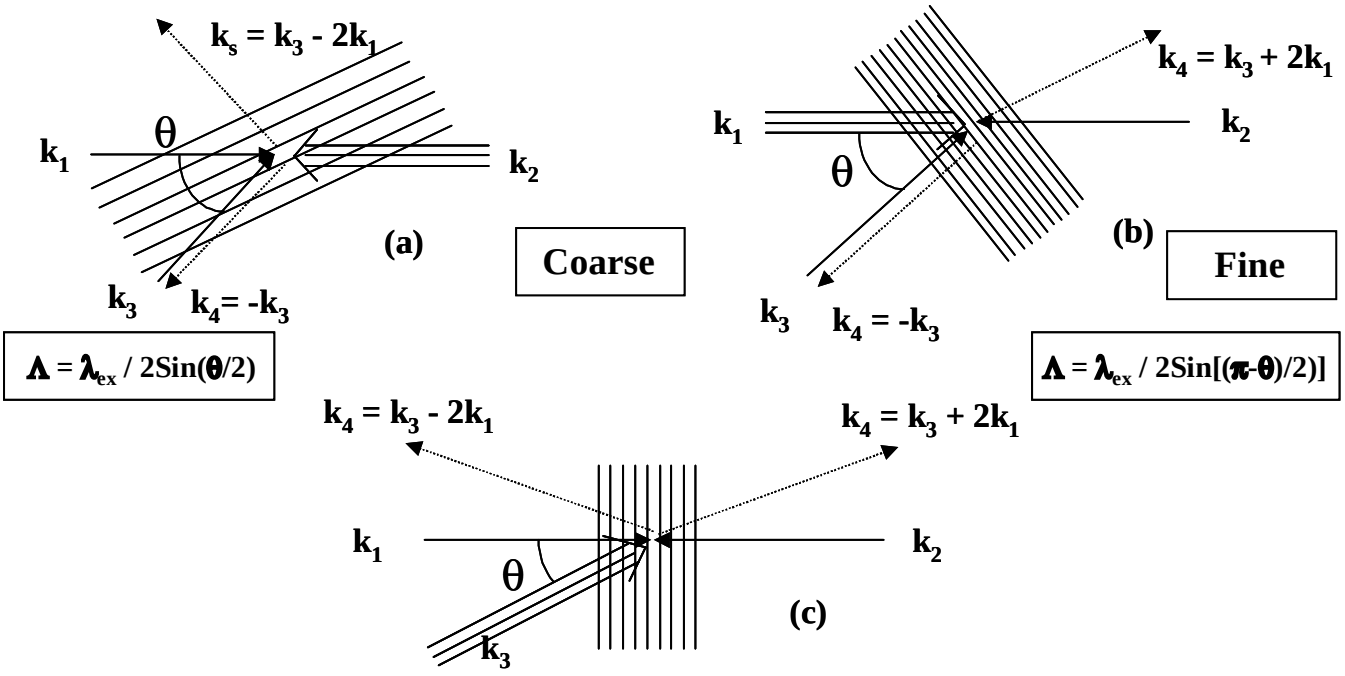

Fig. 2.1 Different gratings formed with interference of any two beams

The applications of Four-Wave Mixing (FWM) can be divided into three categories. First, the creation of a dynamic grating via a material excitation and the subsequent probing of the grating using another beam allow us to study the material excitation processes. Such a spectroscopic technique is versatile and extremely powerful, and has found many applications in various disciplines [17,18]. Second, under specific conditions with the creation of a static grating, the output of FWM is a phase-conjugate (PC) signal. This is the real time holography and can be used in real-time image construction in different applications like optical image and data processing. Third, the possible generation of new frequency components in FWM permits the extension of coherent light sources to new frequency regions in the IR, UV, and XUV where there are not many available.

2.2 Degenerate Four Wave Mixing with Incoherent Light (DFWM-IL)

2.2.1 Characterisation of the Broadband Dye Laser

The source for incoherent light for all the experiments is a home-built broad band dye laser [19]. The versatility and utility of organic dye lasers in science and technology continue to increase even long after the inception of the dye laser. High average power and narrow pulse width dye lasers are developed for spectroscopic studies, communications, atmospheric propagation studies, isotope separation and many other applications. New laser dyes are also being developed which provide high efficiency, designed at low cost and chemical stability for dye lasers at wavelengths ranging from the near infrared to the ultraviolet. Construction and operation of organic dye lasers depend on the photo-physical and chemical properties of the dye solutions, which are used as the gain medium. The structural and spectroscopic properties of efficient laser dyes and detailed information on their lasing properties are listed in the data sheets of dye manufacturers [20]. The most important criteria in selecting components for the dye laser system are the chemical inertness and the construction materials. The safest materials that can be used are glass or quartz, stainless steel and Teflon. One of the most attractive properties of the dye laser is its tunability. The emission spectra of fluorescent dyes are broad permitting the lasing

wavelength to be tuned to any chosen value within a broad range. Moreover the number of fluorescent dyes is very large and different compounds can be chosen for emission over the entire spectral range. Rhodamine 6G and Rhodamine B are still the best dyes available for laser applications. Some of the important parameters related to these dyes are detailed in reference [20].

Fig. 2.2 shows the schematic of the dye laser set-up used for different studies. It has an oscillator and a single stage amplifier. Rhodamine B (RhB) in methanol (107 mg/lit) is used as the gain medium and a pump is used to circulate the liquid (at the rate of 1 litre/minute) to minimise the laser scattering and reduce the possibility of decomposition during the experiment. 8% of the frequency doubled Nd: YAG (Continuum 660 B-10, 532 nm, 10 Hz, 6 ns FWHM, 100 mJ/pulse) laser power split by a plane glass plate, is first expanded by a plano-concave lens of f ~ 50 mm and then focused by a cylindrical lens of f ~ 50 mm into the dye cell of approximately 3 mm (diameter) X 15 mm (length) dimensions. The oscillator cavity consists of a 100% R mirror and ~ 8% R glass plate which produces output of maximum bandwidth. The total length of the oscillator cavity is ~ 17 cm. With both the high reflectivity mirror and the output coupler window being parallel, the resonator cavity is barely stable and hence the alignment has to be made very carefully to avoid any spurious feedback and intensity fluctuations. Necessary care is taken to avoid mechanisms leading to the formation of cavity modes, which leads to undesirable structure in the laser spectrum. The output pulses from the oscillator are amplified using the remaining 92% of the power. Concentration of solution used for amplification is 37.4 mg/lit. The maximum average power that could be achieved after amplification is ~ 20 mW. The output has a FWHM of ~ 7 - 8 nm [fig. 2.3 (a)] and the corresponding τ_c calculated, from the relation $\Delta\nu*\tau_c \sim 1$, is ~ 170 fs. The auto-correlation function obtained by recording the PC signal, as a function of beam 3 delay, in the sample Rhodamine B (in methanol) is shown in fig. 2.3 (b).

If the mirror in the cavity is replaced by a highly dispersive element like a high-resolution grating the spectral width is decreased thereby increasing the

(a)

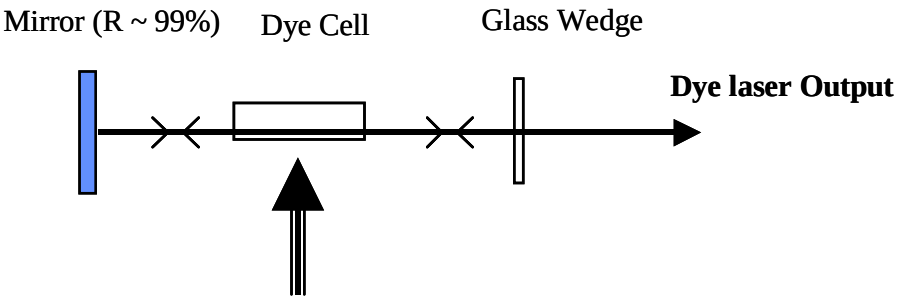

(b)

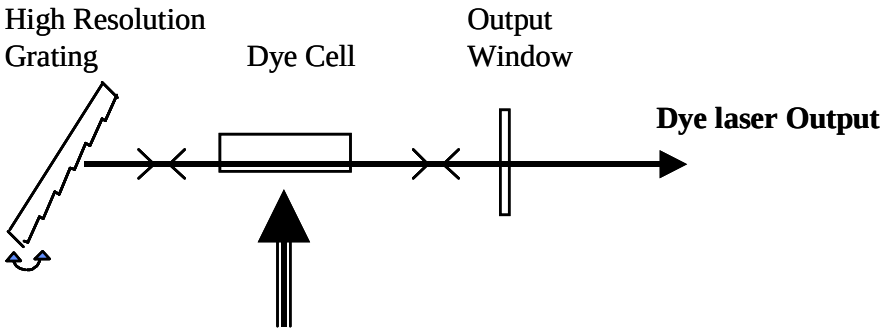

Fig. 2.2 Home built dye laser with (a) Mirror and (b) Grating as tuning elements.

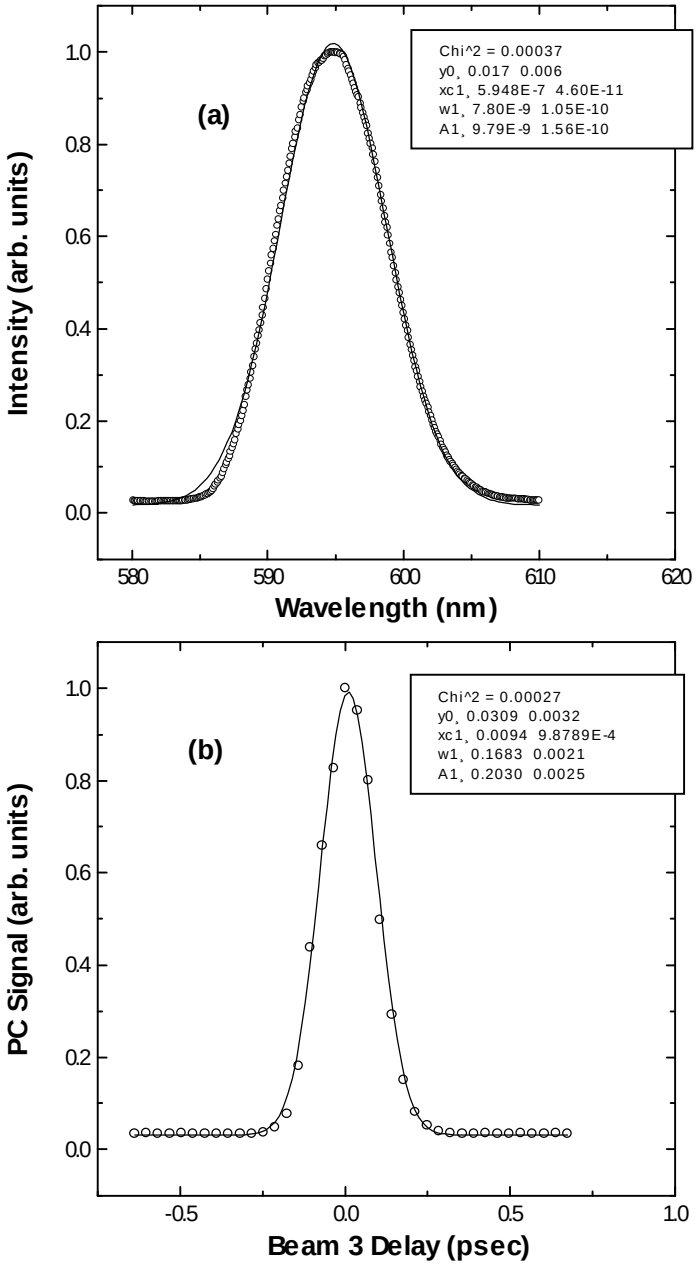

Fig. 2.3 (a) Emission Spectrum of the dye RhB (in methanol). Open circles are experimental data and the line is a fit to gaussian with a width of 7.8 nm **(b)** Autocorrelation function : Time - resolved signal in the same solution. Solid line is a fit to gaussian of width ~ 168 fs

correlation time of the pulses. The grating used in our configuration for tuning the dye laser is a reflection type holographic grating (Bausch and Lomb) with 600 grooves/mm and blazed at 54^0. It has five orders of diffraction and is oriented in the Littrow position [21], for which the incident light and the diffracted light of a given wavelength lie along the same direction. The spectral line narrowing, in the ns pulse, is avoided by using a glass plate of 8% R as output coupler, which also limits the number of passes in the cavity during the short excitation time (6 ns). The spectral recording of the output laser with the grating in cavity is shown in fig. 2.4 (a). The PC signal obtained in the sample RhB with grating in the cavity is shown in fig. 2.4 (b).

2.2.2 Phase-Conjugate Configuration

Figure 2.5 shows the complete details of the degenerate four-wave mixing (DFWM) experimental set-up using incoherent light. The beam is initially collimated using two convex lenses and an aperture is used to cut the scattered background before splitting it into three beams. Two beam splitters (30-70, 50-50) are used to obtain three beams of almost equal intensity. All the three beams have a diameter of ~ 2.5 - 3 mm and could be varied further with an aperture. In the phase conjugate configuration, beam 1 is fixed whereas beams 2 and 3 pass through variable delays. Beam 1 ($\mathbf{k_1}$) is designated as forward pump, beam 2 ($\mathbf{k_2}$) is backward pump and beam 3 ($\mathbf{k_3}$) is the probe. Beam 2 passes through a variable delay (either a micrometer screw or an optical bench, both of which are controlled manually). Beam 3 passes through another delay line mounted on a micrometer screw and connected to a stepper motor, which is controlled with a PC. The maximum resolution we could achieve in both the cases is ~ 5 μ corresponding to 33 fs in time (with a retro-reflector it will be twice the actual path length). The angle between the forward pump and the probe is ~ 10 – 15°. All the beams are focused into the sample contained in 1-mm thick quartz/glass cell using lenses of focal length of ~ 20 cm.

Beam waist at the focus is estimated to be ~ 80 -100 μ (using the formula $4\mathbf{f}\lambda/\pi\mathbf{D}$, where **f** is the focal length of the lens, λ is the wavelength, and **D** is the input

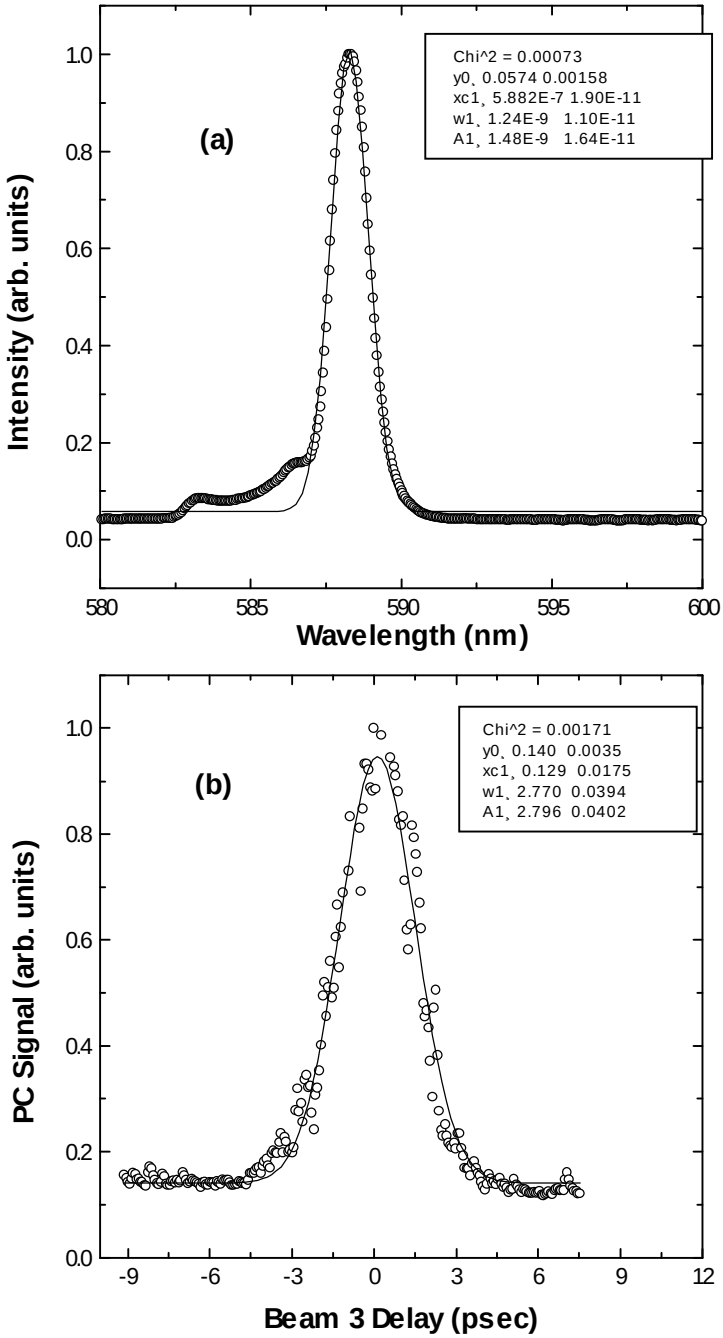

Fig. 2.4 (a) Emission spectrum of the dye laser with grating in the cavity. Solid line is fit to a gaussian. **(b)** PC Signal in the sample CS_2. No decay observed and solid line is fit to gaussian of width 2.78 psec.

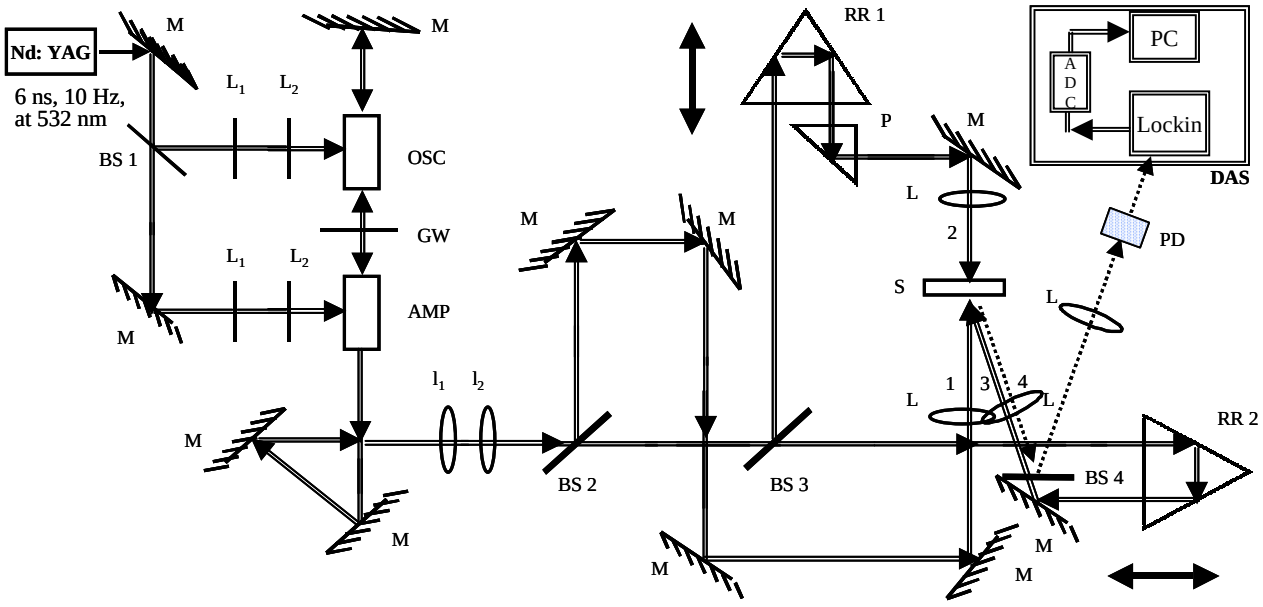

Fig. 2.5 Experimental setup for Degenerate Four Wave Mixing with Incoherent Light

beam diameter. The beam waist measured using a knife-edge technique, at low power densities of the laser beam, is ~ 70 μ. The polarisation state of each individual beam is controlled using a Half Wave Plate (HWP). Proper care is taken to ensure that the counter-propagating and the probe beams are overlapped in the sample, both spatially and temporally. Using a pinhole at the sample position and maximising the transmission through pinhole facilitates spatial alignment. Temporal overlap is accomplished by varying the path length of each of the beams to maximise the PC signal in a standard sample like CS_2 or RhB.

The phase conjugate signal (in $-\mathbf{k}_3$ direction) is isolated using a beam splitter and is passed through an aperture (to reduce the scattered background) and focused on to a fast photodiode (FND 100, rise time ~ 1 ns). Various neutral density filters (NDF) are used for attenuating the probe and the signal beams. The signal collected using a fast photodiode (PD, FND 100, rise time ~ 2 ns) is observed on a large bandwidth oscilloscope (Tektronix 2465 B, 400 MHz or Tektronix TDS 210, 60 MHz) to ensure the PD does not get saturated. (In the initial stages of the present work the signal is recorded using a Digitising Camera System [TEK], which records the pulse trace onto the PC and the averaging is done using the PC software). This effect is clearly seen in the signals obtained in the samples Zinc meso-tetraphenyl porphyrin (ZnmTPP), Zinc meso-tetra- (p-methoxyphenyl) tetrabenzporphyrin (ZnmpTBP) in the initial stages and other porphyrins in the later stages. In the later stages the signal is fed to a lock-in amplifier (SRS 830) and to the ADC card where it is averaged several times (typical averages are ~ 300). The output of the ADC card finally gets recorded in a PC. A GWBASIC program performs the stepper motor movement and the data averaging simultaneously.

2.2.3 Boxcar Configuration

For the Boxcar configuration, the same set-up is retained with slight modifications. The second beam is diverted using another retro-reflector and it comes parallel to the first beam but at lesser height than the first beam. Since the probe and forward pump are in same plane, the second beam forms the third corner of the square

and the signal is seen at the fourth corner of the square. Schematic of the set-up is shown in fig. 2.6. The delays of beams 2 and 3 could be varied using the stepper motor. Observing and optimising the diffracted signals, in both horizontal and vertical directions, ensured the zero delay of different beams. The signal(s) obtained are spatially filtered before being fed to the fast PD to lock-in and to ADC which finally gets recorded in the computer.

2.2.4 Self-Diffraction Configuration

In the self-diffraction/forward four-wave mixing configuration the backward pump beam is blocked and the signals are obtained aligning the beams 1 and 3. The angle between the forward pump ($\mathbf{k_1}$) and probe beams ($\mathbf{k_2}$) is ~ 5 - 10^0 and the first order diffracted signals are obtained in $2\mathbf{k_1} - \mathbf{k_2}$ and $2\mathbf{k_2} - \mathbf{k_1}$ directions, as shown in fig. 2.7, due to the third order nonlinearity. Beams 3, which is the probe passes through variable delay, as described above, and the signal(s) is (are) collected using similar Photodiodes. The signals and recorded as a function of the delay of beam 3.

2.3 Degenerate Four-Wave Mixing with 35 ps pulses (DFWM-PS)

The experimental set-up for the $\chi^{(3)}$ measurements and time-delayed four wave mixing using the ps pulses is shown in fig. 2.8. The input beam is from a hybrid mode-locked Nd: YAG laser emitting 532 nm and the pulses are of 35 ps duration at 10 Hz. The maximum pulse energy is ~ 30 mJ. The input beam is passed through an aperture to get a spatially filtered beam of ~ 7 mm diameter. Using a beam splitter a part of it is split and used for the backward pump (beam 3, which goes through a microprocessor controlled, high precision delay line) and is focused using a 1m lens. The rest of the beam is again split using another beam splitter. The second beam, which is the probe, (beam 2) goes through a delay line (micrometer screw) and comes at an angle to the forward pump. Beam 1 (forward pump) reaches the sample at a fixed delay and is focused onto the sample using a 2m focal length lens. All the beams have Neutral Density Filters in their paths to change the intensities accordingly. The angle between the forward pump (beam 1) and the probe (beam 2)

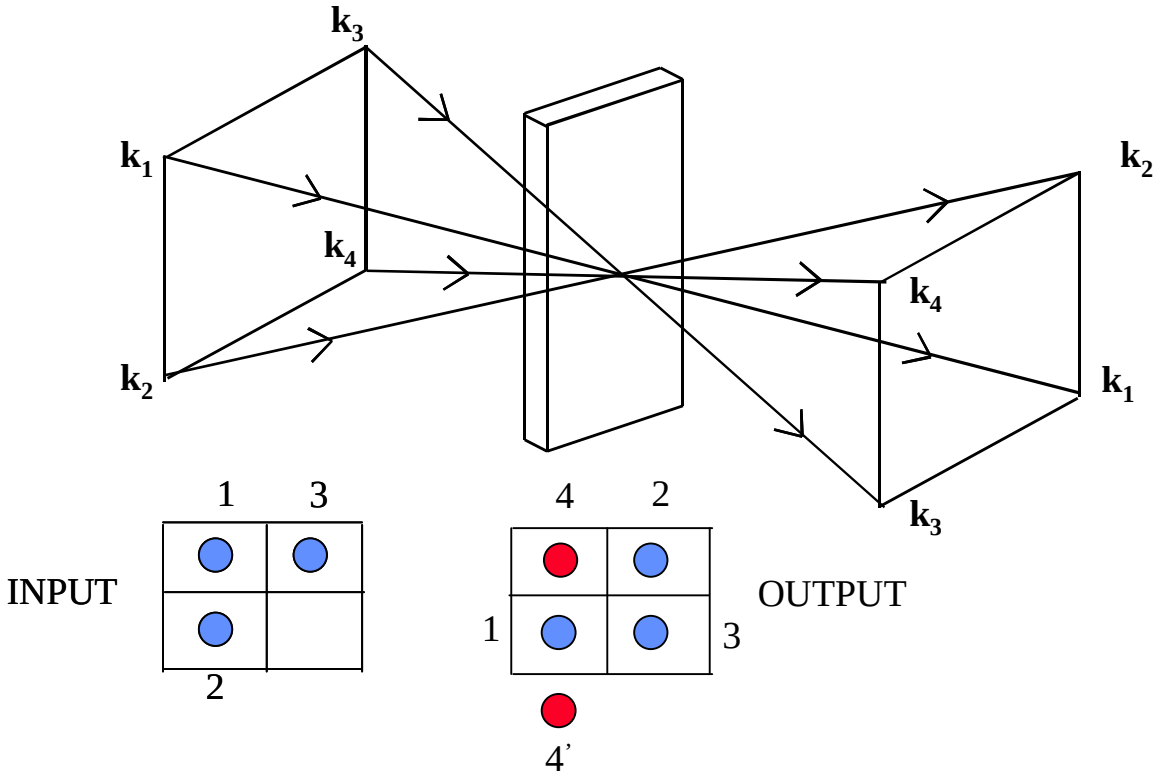

Fig. 2.6 DFWM set-up in the boxcar configuration. 4 and 4' are the signals

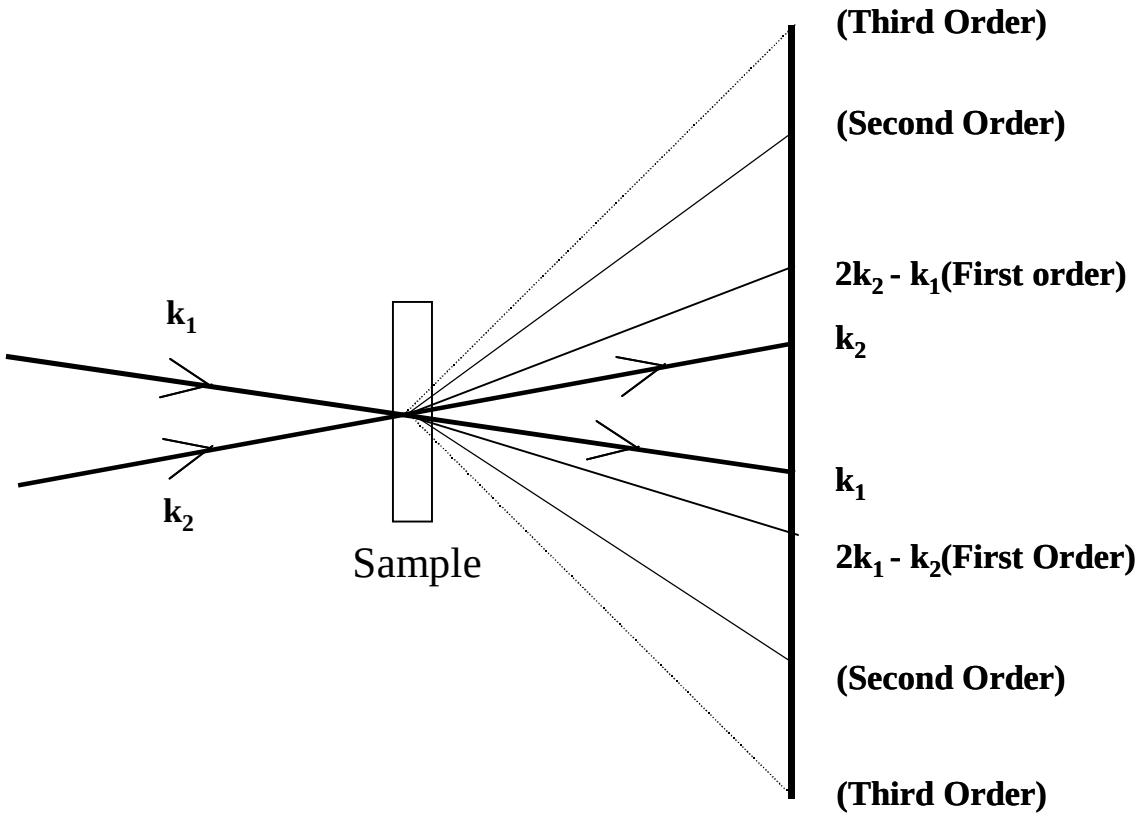

Fig. 2.7 Experimental setup for the Forward Four Wave Mixing

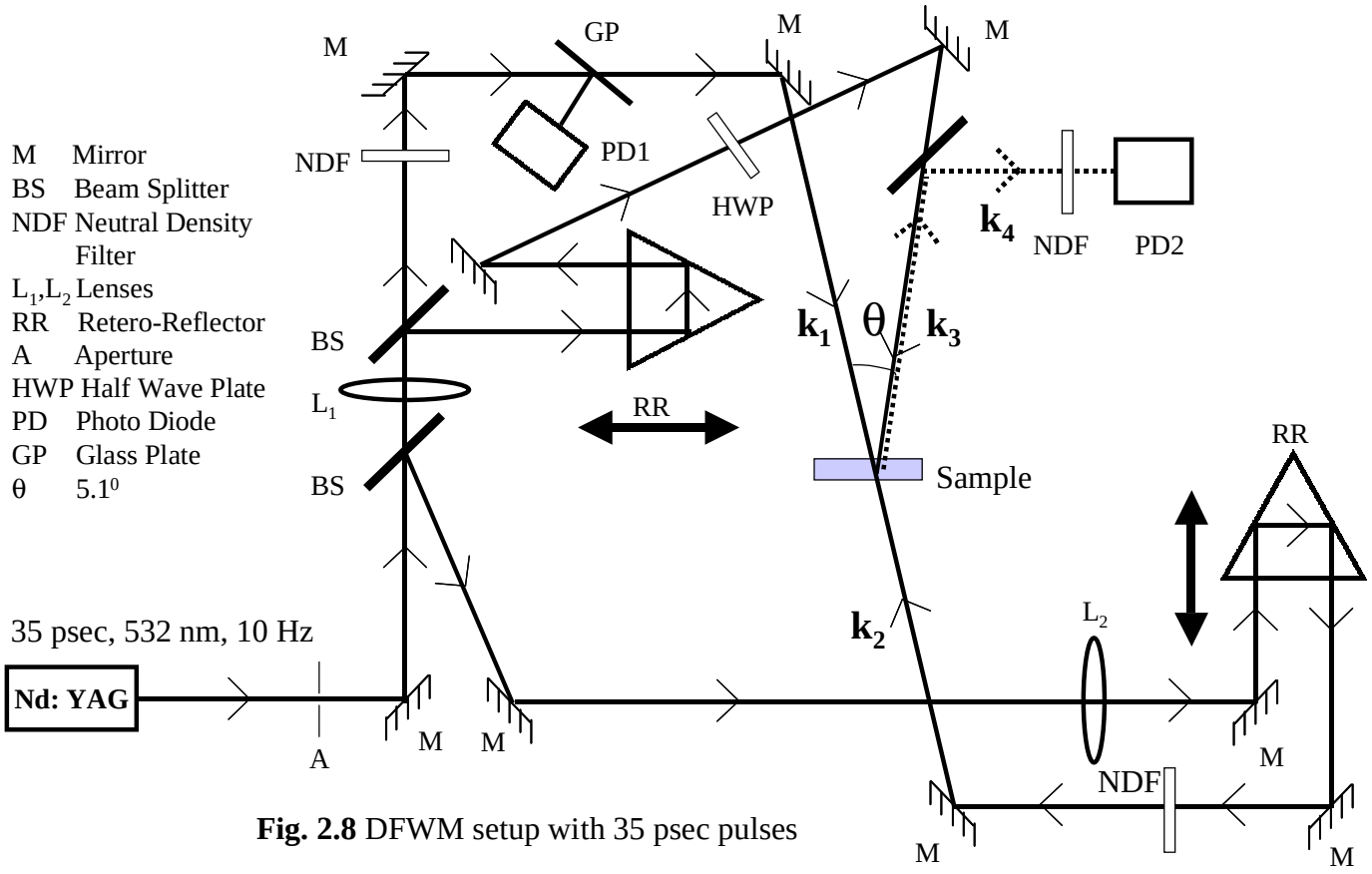

Fig. 2.8 DFWM setup with 35 psec pulses

is measured to be ~ 5.1^0. A half wave plate (HWP) is introduced in the probe beam to change its state of polarisation. A part of the forward pump is picked up by a photodiode (NRC 818J-09B) to monitor the pulse to pulse fluctuations. All the samples, in the form of solution, are placed in a 1-mm quartz/glass cuvette.

2.4 Z-Scan

2.4.1 Closed aperture scan for sign and refractive nonlinearity

The Z-scan technique is a simple, sensitive, single beam method that uses the principle of spatial beam distortion to measure both the sign and the magnitude of refractive nonlinearities of optical materials. The experiment uses a Gaussian beam from a laser in tight focus geometry to measure the transmittance of a nonlinear medium through a finite aperture in the far field as a function of the sample position z, from the focal plane. In addition to this, the sample transmittance without an aperture is also measured to extract complementary information about the absorptive nonlinearities of the sample. The transmittance characteristics of the sample with a finite aperture depend on the nonlinear refractive index, as elucidated below.

Consider, for instance, a material with a negative nonlinear refraction and of thickness smaller than the diffraction length ($\pi\omega_0^2/\lambda$) of the focused beam being positioned at various positions along the Z-axis (fig. 2.9). This situation can be regarded as treating the sample as a thin lens of variable focal length due to the change in the refractive index at each position ($\mathbf{n = n_0 + n_2 I}$). When the sample is far from the focus and closer to the lens, the irradiance is low and the transmittance characteristics are linear. Hence the transmittance through the aperture is fairly constant in this region. As the sample is moved closer to the focus, the irradiance increases inducing a negative lensing effect. A negative lens before the focus tends to collimate the beam. This causes the beam narrowing leading to an increase in the measured transmittance at the aperture. A negative lens after the focus tends to diverge the beam resulting in the decrease of transmittance. As the sample is moved far away from the focus, the transmittance becomes linear in Z as the irradiance becomes low again. Thus the curve

for Z versus transmittance has a peak followed by a valley for a negative refractive nonlinearity. The curve for a positive refractive nonlinearity will give rise to the opposite effect, i.e. a valley followed by a peak. This technique has several *advantages*, some of which are

- Simplicity: No complicated alignment except for keeping the beam centered on aperture.
- Simultaneous measurement of both sign and magnitude of nonlinearity.
- Data analysis is quick and simple except for some particular conditions.
- Possible to isolate the refractive and absorptive parts of nonlinearity unlike in DFWM.
- High sensitivity, capable of resolving a phase distortion of $\lambda/300$ provided the sample is of high optical quality.
- Close similarity between the Z-scan the Optical Power Limiting geometry.

Some of the *disadvantages* include

- Stringent requirement of high quality Gaussian TEM_{00} beam for absolute measurements.
- For non-Gaussian beams the analysis is completely different. Relative measurements against a standard samples allows relaxation on requirements of beam shape
- Beam walk-off due to sample imperfections, tilt or distortions.
- Not suitable for measurement of off-diagonal elements of the susceptibility tensor except when a second non-degenerate frequency beam is employed.

The Z-scan technique has been used extensively to study different materials like semiconductors, nano-crystals, semiconductor-doped glasses, liquid crystals, organic materials, biomaterials etc. To enhance it's sensitivity and applicability new extensions have been added. A two color Z-scan is used to perform the studies of non-degenerate optical nonlinearities. A much more sensitive technique, EZ-scan (eclipsed Z-scan), has been developed which utilizes the fact that the wings of a circular Gaussian beam are much more sensitive to the far-field beam distortion. A reflection Z-scan technique

was introduced to study the optical nonlinearities of surfaces. Z-scan with top-hat beams, elliptical Gaussian beams have been performed resulting in better sensitivity. The dual wavelength (two-color) extension of the standard Z-scan technique has been used to measure the non-degenerate nonlinearities. This has been further used to time-resolve the dynamics of the nonlinear process by introducing a delay between the pump and probe beams. A comprehensive review of different techniques of Z-scan could be found in any of the references listed in [22].

2.4.2 Open aperture scan for absorptive nonlinearity

In the above discussion a purely refractive nonlinearity was considered assuming that absorptive nonlinearities are absent. The presence of multi-photon (two or more) absorption suppresses the peak and enhances the valley, while saturation of absorption produces the opposite effect. The sensitivity of the experiment to refractive nonlinearities is entirely due to the aperture. The removal of the aperture will make the Z-scan sensitive to absorptive nonlinearities alone. Thus by doing the Z-scan with and without aperture both the refractive and absorptive nonlinearities of the sample can be studied. Z-scan studies of the all the samples are performed using broadband source / ns pulses / ps pulses. The details of the experimental set-up are shown in fig. 2.9. Spatially filtered input beam is focused using a lens of focal length ~ 80 mm. For Z-scan with ps pulses a longer focal length lens is used since the peak intensities are large compared to ns pulses. The sample placed in a 1-mm cuvette is scanned across the focus using a stepper motor controlled by PC. A part of the input beam split using a glass plate is monitored using a PD. The transmitted light is then collected using another lens (large area) of f ~ 100 mm and another fast photodiode. The output beam is again split using a beam splitter. For the closed aperture Z-scans an aperture of known size is placed after the cell and the light passing through the aperture is collected using a similar photo-diode. Different neutral density filters are used for attenuation of the transmitted beam to ensure that the photodiode does not get saturated. The photodiode output is fed to a lock-in amplifier (SRS 830 or Princeton Applied Research) and finally gets recorded

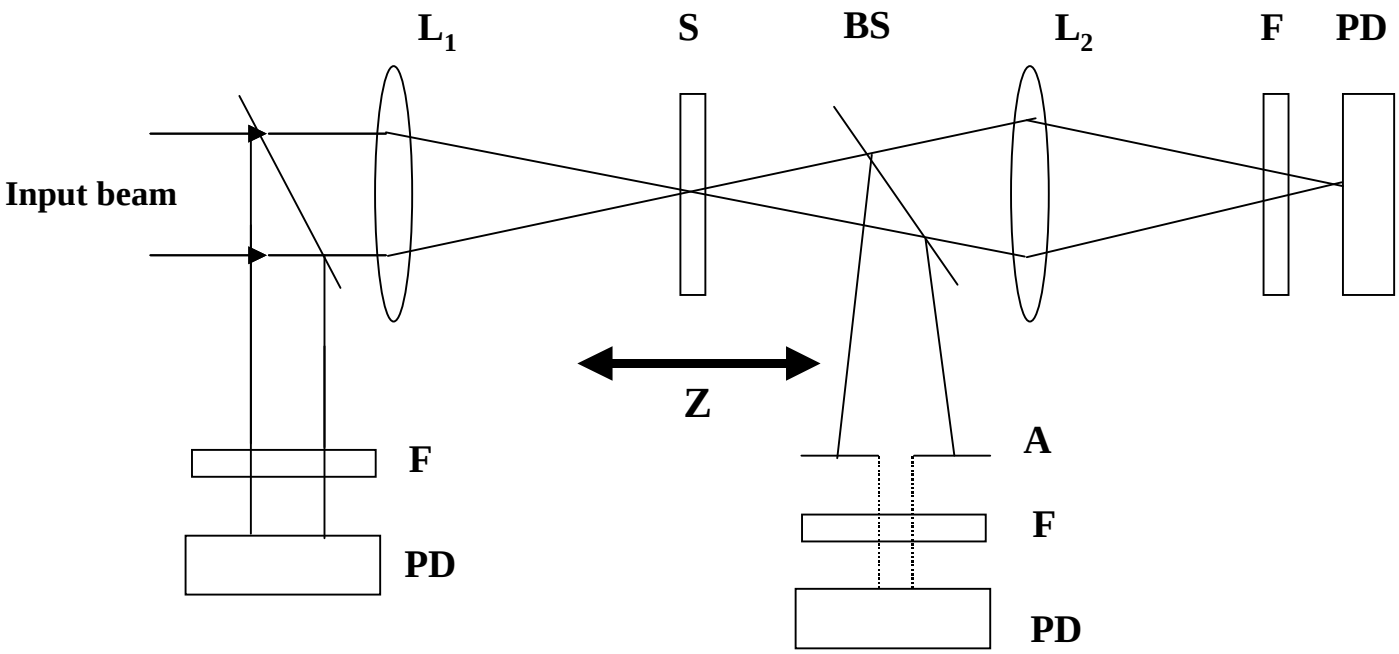

L_1, L_2 - Lenses S - Sample BS - 50-50 beam splitter
F - Neutral density filter A - Aperture PD - Photodiode

Fig. 2.9 Z-scan (closed and open aperture) experimental setup.

in a PC. The output data is averaged several times (typical number of averages is 300). The step size used is 0.25 / 0.5 mm.

2.5 Photo-physics of a typical organic molecule

In molecules, the absorption of electromagnetic radiation results in the excitation of an electron from a lower to a higher molecular quantum state. The electronically excited molecule is energetically unstable with respect to ground state. If the molecule does not rearrange or fragment it will find some way of losing its excitation energy to the ground state. In fact, there are number of different possible de-excitation pathways and the ones that are most favourable depend on the type of molecule and the nature of electronic states involved [23]. The de-excitation pathways are often characterised by very rapid rates. One of the most interesting properties of electronically excited molecules is their tendency to re-emit radiation on returning to the ground state. The absorption of ultraviolet or visible light by an organic molecule causes the excitation of an electron from an initially occupied, low energy orbital to a high energy, unoccupied orbital. The energy of the absorbed photon is used to energise an electron and cause it to jump to a higher energy orbital. Two excited electronic states derive from the electronic orbital configuration produced by light absorption. In one state, the electron spins are paired (anti-parallel) and in the other state the electron spins are unpaired (parallel). The state with paired spins has no resultant spin magnetic moment. A state with paired spins remains a single state in the presence of a (laboratory) magnetic field, and is termed as singlet state. A state with unpaired spins interacts with a (laboratory) magnetic field and splits into three quantized states, and is termed as triplet state. An energy diagram is a display of the relative energies of the ground state, the excited singlet states, and triplet states of a molecule for a given, fixed nuclear geometry.

An energy level diagram characteristic of a typical organic dye molecule is shown in fig. 2.10. The electronic ground state of the molecule is a singlet state, designated as S_0, which spans a range of energies determined by the quantized vibrational and rotational excitation of the molecule. The typical energy between the

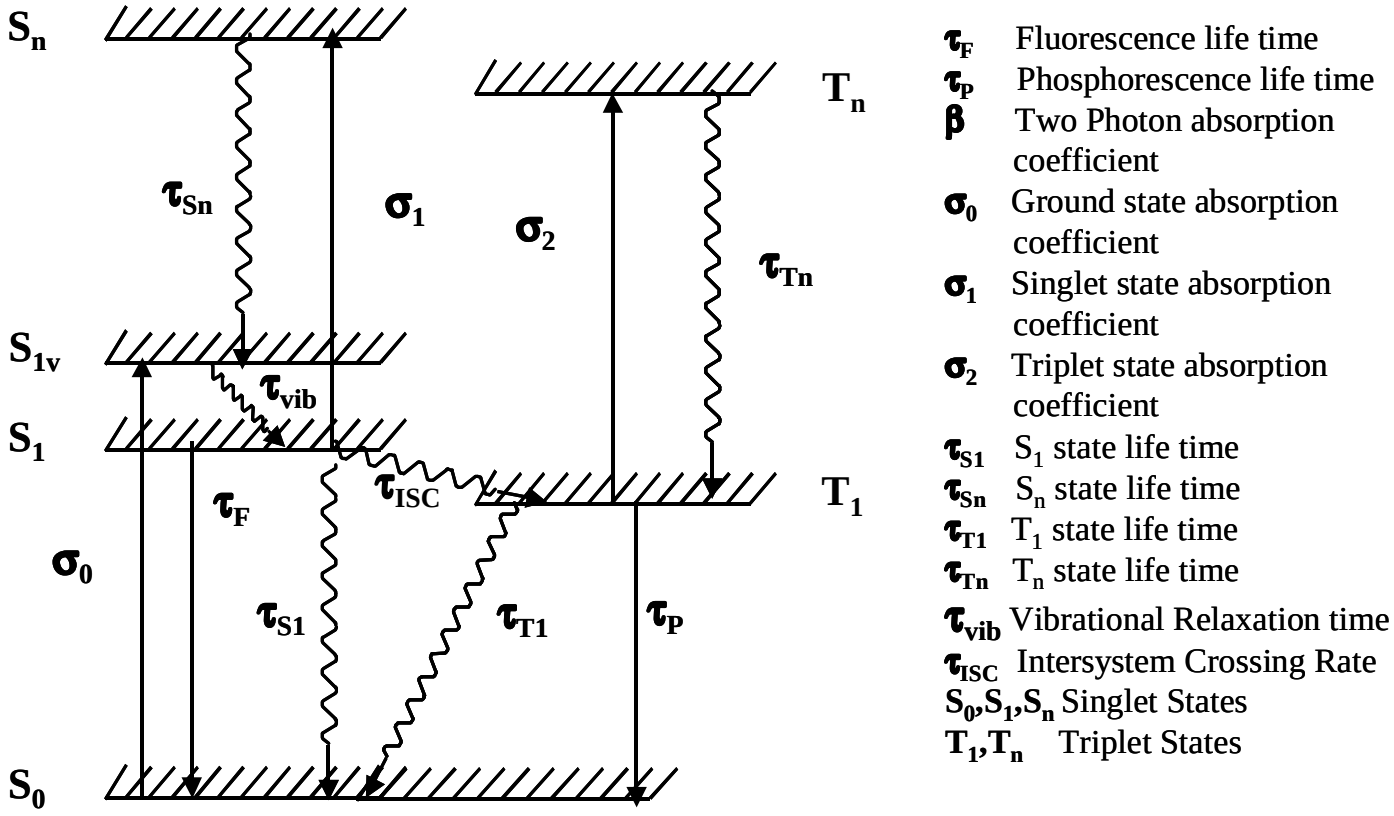

Fig. 2.10 Energy level diagram of a typical organic molecule

vibrational levels is of the order of 100 cm^{-1}. The rotational levels provide a near continuum of states between the vibrational levels. The higher singlet states are denoted as S_1 and S_n. Each electronic state has similar broad continuum of levels and the optical transitions between these continua leads to broad absorption and emission spectra. Transition between singlet states are spin-allowed, giving rise to strong absorption bands. When a laser pulse is incident, the molecules are excited from the lowest levels of the ground state S_1 to the highest vibrational states of S_1 (S_{1v}). The decay from S_{1v} to S_{10} is non-radiative and occurs within few ps. From S_{10} the molecules can relax back to the ground state radiatively or non-radiatively to the ground state or crossover to the triplet state (Intersystem Crossing). The radiative decay, which is spontaneous, from S_{10} to S_0 is known as **Fluorescence** and is governed by the lifetime of the S_1 state. For organic molecules the lifetime is typically of the order of few ns. The energy difference between absorption and emission processes is taken by the non-radiative decay in the S_1 and S_0 states and the relaxation of the molecules from S_{10} to the lowest triplet state T_1 is governed by the intersystem crossing rate. The intersystem crossing rate constant is typically 10^{11} to 10^7 s^{-1} due to spin restriction factor. Another important process of de-activation of the S_1 state is the **Internal Conversion,** which is the non-radiative decay of S_{10} to S_0. The decay from T_1 to S_0 can be radiative or non-radiative and is termed as **Phosphorescence** if it is the former type. Typical phosphorescence life times are in the range of ms to μs. The lifetime of the triplet state T_1 is generally large since the triplet-singlet transition is dipole forbidden.

In the first excited singlet and triplet states, under special experimental conditions (higher intensities), the molecule may be promoted to the higher states S_n and T_n respectively. These higher states relax back to the S_1 and T_1 on a very fast time scale (few hundred fs) and in the process generate a vibrationally excited state (Kasha's rule). Higher triplets can also be populated by intersystem crossing from higher singlet states if the rate constants are competitive for internal conversion and intersystem crossing in the upper states. Thus, although direct absorption from ground singlet to triplet state is forbidden by selection rules, it can be populated indirectly. We will be using vibrational relaxation time also to represent the dephasing time for the S_n

and S_1 states. This is so because of band of vibrational levels, closely spaced, in the S_n states leading to very fast dephasing time $\mathbf{T_2}$. Since the vibrational levels in S_1 state are far more separated the dephasing ($\boldsymbol{\tau_{vib}}$) is expected to slow compared to the S_n states.

2.6 Results on the samples Rhodamine B and CS_2

Standard samples of CS_2 and RhB are studied in order to test the validity of the present Incoherent Laser Spectroscopy technique to measure the ns and ps relaxation times through DFWM. In the first stage we studied the dynamics of RhB dissolved in methanol. The phase conjugate signal recorded as a function of delay of beam 3, with beam 2 delay at zero, is shown in fig. 2.3 (b). The curve obtained is a symmetric one with no decay observed for both positive and negative delays (convention used throughout the thesis is, if pulse arrives in the sample early it is denoted as negative delay and if it arrives late it is denoted as positive delay). Since the phase relaxation in such dyes is very fast, typically less then 100 fs [24], we do not observe any decay in the profile. In other words the curve we observed was just the auto-correlation curve. Beyond 170 fs delay time (FWHM of the curve) no two pulses are correlated and hence there is no signal. Background signal consists of the scattered light collected by the photo-diode. τ_c obtained from the theoretical calculations agrees very well with experimental value.

In the second stage we studied the relaxation times in liquid CS_2. CS_2 is one of the most familiar and simplest optical Kerr media. Fig. 2.11 (a) depicts the signal in CS_2 (open circles) and it is found to be asymmetric with three components having different life times. The intense component is due to the coherence spike as it coincides with the auto-correlation function (solid line). There are two more components with short and the long decay times. Figure 2.11 (b) shows the values obtained through least squared fitting of the data (**0.22 ps** for the short component and **2.2 ps** for the long component). Ps and sub-ps relaxation times measurement of the optical Kerr effect was done with more accuracy with the advent of ps/fs laser systems. The ps relaxation in CS_2 is considered to be associated with orientational

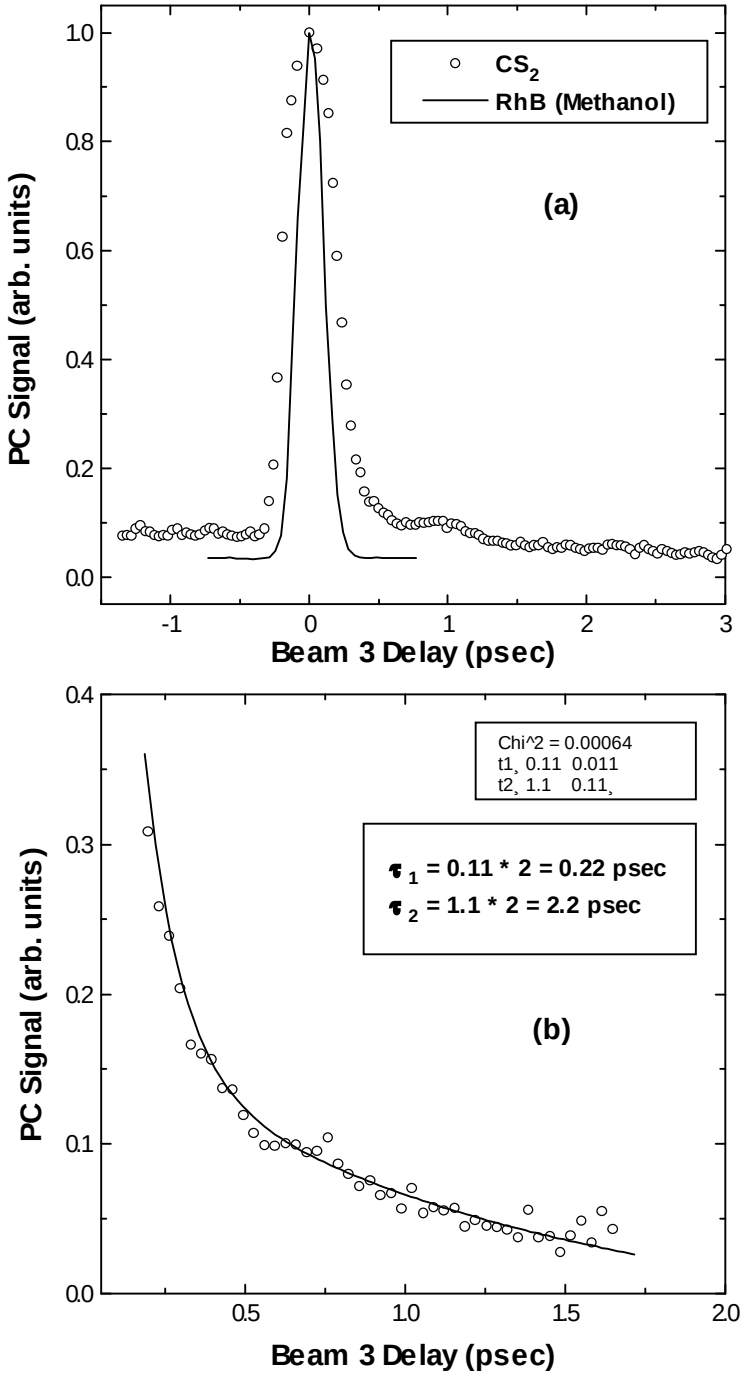

Fig. 2.11(a) The time-resolved signals obtained for CS_2 and RhB (methanol). **(b)** Double exponential fit of the PC Signal. The two lifetimes are **0.22 psec** and **2.2 psec.** Open circles are data and the line is the fit.

randomisation by rotational diffusion of molecules subsequent to their alignment by an external electric field. Several mechanisms have been proposed [25] to explain the sub-ps response like the a) damped librational motion, b) the time dependant behaviour resulting from collisions which induce an anisotropic polarizability in colliding pairs of atoms or molecules, c) short time behaviour associated with the rotational diffusion motion of molecules possessing a large anisotropic polarizability etc. Our values match perfectly with most of the reported values proving the validity of the present set-up for the measurement of different relaxation times.

2.7 Conclusions

1. The home-built dye laser with different elements (mirror and grating) in the cavity has been tried and the resulting broadband laser pulses are used for different DFWM and Z-scan experiments.

2. With RhB as the gain medium and a mirror in the cavity we obtained the correlation time as ~ 170 fs through time-resolved studies as well as from the inverse of bandwidth, obtained through the spectral recording, of the laser pulses.

3. When the mirror is replaced by a high-resolution grating we could get a correlation time of ~ 2.8 ps obtained from the DFWM signal in RhB and CS_2.

4. The initial results of phase relaxation measurements and oreintational relaxation measurements in RhB and CS_2 respectively match very well with those reported in literature thereby calibrating our experimental set-up for the measurement of ps and sub-ps relaxations using an incoherent laser source.

2.8 References

1. Y.R. Shen, *The Principles of Nonlinear Optics*, New York: Wiley, USA, 1984, Chap. 14 - 15; Y.R. Shen, *IEEE J. Quant. Electron.* **22**, 1196, 1986.
2. N. Bloembergan, *Nonlinear Optics*, Benjamin, New York, 1977.
3. M.D. Levenson, *Introduction to Nonlinear Laser Spectroscopy*, New York: Academic, 1982
4. R.A. Fischer, *Optical Phase Conjugation*, New York: Academic, USA, 1983.
5. H.J. Eichler, P. Gunter, and D.W. Pohl, *Laser-Induced Dynamic Gratings*, Springer-Verlag, Berlin, Heidelberg, Germany, 1986.
6. B.Ya. Zeldovich, N.F. Philipetsky, V.V. Shkunov, *Principles of Phase Conjugation*, Springer series in optical sciences, Vol. 42, Springer, Berlin, Gemany, 1985.
7. D.M. Pepper, Ed. *Opt. Engg.* **21,** 2, 1982.
8. A.D. Walser, G. Coskun, and R. Dorsinville, *Electrical and Optical Polymer Systems*, ed.'s D.L. Wise, G.E. Wnek, D.J. Trantolo, T.M. Cooper, and J.D. Gresser, Marcel Deccer Inc., New York, 423-452.
9. M. Zhao, Y. Cui, M. Samoc, P.N. Prasad, M.R. Unroe, and B.A. Reinhardt, *J. Chem. Phys.* **95,** 3991, 1991; S.K. Ghoshal, P. Chopra, B.P. Singh, J. Swiatkiewicz, and P.N. Prasad, *J. Chem. Phys.* **90**, 5078, 1989.
10. M. –T. Zhao, B.P.Singh, and P.N. Prasad, *J. Chem. Phys.* **89,** 5535, 1988.
11. B.P. Singh, M. Samoc, H.S. Nalwa, and P.N. Prasad, *J. Chem. Phys.* **92**, 2756, 1990.
12. Y. Pang, M. Samoc, and P.N. Prasad, *J. Chem. Phys.* **94**, 5282, 1991.
13. B.P. Singh, P.N. Prasad, and F.E. Karasz, *Polymer* **29**, 1940, 1988.
14. M. Samoc and P.N. Prasad, *J. Chem. Phys.* **91**, 6643, 1989.
15. Y. Cui, M. Zhao, G.S. He and P.N. Prasad, *J. Phys. Chem.* **95**, 6842, 1991.
16. M.K. Casstevens, M. Samoc, J. Pfleger, and P.N. Prasad, *J. Chem. Phys.* **92**, 2019, 1990.
17. R.R. Rojo, Ph.D. Thesis, Heriott-Watt University, April 1994, UK.
18. F.J. Aranda, Ph.D. Thesis, University of Massachusetts, Lowell, USA, 1995.
19. V.N. Kumar, Ph.D. Thesis, University of Hyderabad, January 1997.

20. M. Maeda, Laser Dyes, Academic Press, New York, 1984; U. Brackmann, Lambda Chrome Laser Dyes, Lambda Physik, Gottingen, 1986.
21. G. Yamaguchi, F. Endo, S. Murakawa, S. Okamura, and C. Yamanaka, *Japn. J. Appl. Phys.* **7**, 179, 1968**;** F.P. Schafer, in *Dye Lasers*, F.P. Schafer Ed., Springer Verlag, 1977; F.P. Schafer, *Liquid Lasers* in Laser handbook, Edited by F.T. Areechi and E.O. Schulz-Dubois (North-Holland, 1972), Vol. 1.
22. P.B. Chapple, J.M. Staromlynska, J.A. Hermann, and T.J. McKay, *J. Nonlinear Opt. Phys. and Mat.* **3**, 251, 1997; T. Xin, D.J. Hagan, M. Sheik-Bahae, and E.W. Van Stryland, *Opt. Lett.* **19**, 317, 1994; D.V. Petrov, *J. Opt. Soc. Am.* **B13**, 1491, 1996; J. –G. Tian, W. –P. Zang, and G. Zhang, *Opt. Commun.* **107**, 415, 1994; S.M. Mian, B. Taheri, and J.P. Wicksted, *J. Opt. Soc. Am.* **B13**, 856, 1996 (and references therein); M. Sheik-Bahae, A.A. Said, D.J. Hagan, M.J. Soileau, and E.W. Van Stryland, *Opt. Engg.* **30,** 1228, 1991; S.V.Kershaw, *J. Mod. Opt.* **42**, 1361, 1995.
23. N.J. Turro, "Modern Molecular Photo-Chemistry", The Benjamin/Cummings Publishing Co. Inc., 1978; K.K. Rohatgi-Mukherjee, "Fundamentals of Photo-Chemistry", Wiley Eastern Ltd., New Delhi, 1992.
24. H. Souma, E.J. Heilweil, and R.M. Hochstrasser, *J. Chem. Phys.* **76**, 5693, 1982; A.M. Weiner and E.P. Ippen, *Chem. Phys. Lett.* **114**, 456, 1985; A.M. Weiner, S. De Silvestri, and E.P. Ippen, *J. Opt. Soc. Am.* **B2**, 654, 1985; A. Kummrow and A. Lau, *Appl. Phys.* **B63**, 209, 1996 and references therein
25. C.E. Barker, R. Trebino, A.G. Kostenbauder, and A.E. Stegeman, *J. Chem. Phys.* **92**, 4740, 1990; C. Kalpouzos, W.T. Lotshaw, D. McMorrow, and G.A. Kenney-Wallace, *J. Phys. Chem.* **91**, 2028, 1987; B.I. Greene and R.C. Farrow, *Chem. Phys. Lett.* **98**, 273, 1983; J. Etchepare, G. Grillion, and A. Antonetti, *Chem. Phys. Lett.* **107**, 489, 1984; B.I. Greene and R.C. Farrow, *J. Chem. Phys.* **77**, 4779, 1982; J. -M. Halbout and C.L. Tang, *Appl. Phys. Lett.* **40**, 765, 1982; C.L. Tang and J. -M. Halbout, in *Picosecond Phenomena Vol. 3*, ed.'s K.B. Eisenthal, R.M. Hochstrasser, W. Kaiser, and A. Laubereau, Springer, Berlin, 1983, 212; C.L. Tang and J. -M. Halbout, *Time Resolved Vibrational Spectroscopy*, Academic Press Inc., 73, 1983.